

Mid-infrared dual-comb polarimetry of anisotropic samples

Karsten Hinrichs¹, Brianna Blevins², Andreas Furchner³, Nataraja Yadavalli², Sergiy Minko⁴, Raphael Horvath⁵, and Markus Mangold⁵

¹Leibniz-Institut für Analytische Wissenschaften – ISAS eV Department Berlin

²University of Georgia

³Helmholtz Zentrum Berlin

⁴The University of Georgia

⁵IRsweep AG

October 18, 2022

Abstract

The mid-infrared (mid-IR) anisotropic optical response of a material probes vibrational fingerprints and absorption bands sensitive to order, structure and direction dependent stimuli. Such anisotropic properties play a fundamental role in catalysis, optoelectronic, photonic, polymer and biomedical research and applications. Infrared dual-comb polarimetry (IR-DCP) is introduced as a powerful new spectroscopic method for the analysis of complex dielectric functions and anisotropic samples in the mid-IR range. IR DCP enables novel hyperspectral and time-resolved applications far beyond the technical possibilities of classical Fourier-transform IR (FTIR) approaches. The method unravels structure–spectra relations at high spectral bandwidth (100 cm⁻¹) and short integration times of 65 μs, with previously unattainable time resolutions for spectral IR polarimetric measurements for potential studies of noncyclic and irreversible processes. The polarimetric capabilities of IR-DCP are demonstrated by investigating an anisotropic inhomogeneous free-standing nanofiber scaffold for neural tissue applications. Polarization sensitive multi-angle dual-comb transmission amplitude and absolute phase measurements (separately for ss-, pp-, ps- and sp-polarized light) allow the in-depth probing of the samples' orientation dependent vibrational absorption properties. Mid-IR anisotropies can be quickly identified by cross-polarized IR-DCP polarimetry.

Mid-infrared dual-comb polarimetry of anisotropic samples

Karsten Hinrichs,^{1,*} Brianna Blevins,^{2,3} Andreas Furchner,⁴ Nataraja Sekhar Yadavalli,^{2,3} Sergiy Minko,^{2,3,5} Raphael Horvath,⁶ and Markus Mangold⁶

¹ Leibniz-Institut für Analytische Wissenschaften – ISAS – e.V., Schwarzschildstraße 8, 12489 Berlin, Germany

² Nanostructured Materials Laboratory, The University of Georgia, Athens, Georgia 30602, USA

³ Department of Chemistry, The University of Georgia, Athens, Georgia 30602, USA

⁴ Helmholtz-Zentrum Berlin für Materialien und Energie, Division Energy and Information, Schwarzschildstraße 8, 12489 Berlin, Germany

⁵ Department of Textile, Fiber, and Polymer Sciences, The University of Georgia, Athens, Georgia 30602, USA

⁶ IRsweep AG, Laubisruetistrasse 44, 8712 Staefa, Switzerland

Corresponding author: karsten.hinrichs@isas.de

Abstract

The mid-infrared (mid-IR) anisotropic optical response of a material probes vibrational fingerprints and absorption bands sensitive to order, structure and direction dependent stimuli. Such anisotropic properties play a fundamental role in catalysis, optoelectronic, photonic, polymer and biomedical research and applications. Infrared dual-comb polarimetry (IR-DCP) is introduced as a powerful new spectroscopic method for the analysis of complex dielectric functions and anisotropic samples in the mid-IR range. IR-DCP enables novel hyperspectral and time-resolved applications far beyond the technical possibilities of classical Fourier-transform IR (FTIR) approaches. The method unravels structure–spectra relations at high spectral bandwidth (100 cm^{-1}) and short integration times of $65\text{ }\mu\text{s}$, with previously unattainable time resolutions for spectral IR polarimetric measurements for potential studies of noncyclic and irreversible processes. The polarimetric capabilities of IR-DCP are demonstrated by investigating an anisotropic inhomogeneous free-standing nanofiber scaffold for neural tissue applications. Polarization sensitive multi-angle dual-comb transmission amplitude and absolute phase measurements (separately for ss-, pp-, ps- and sp-polarized light) allow the in-depth probing of the samples' orientation dependent vibrational absorption properties. Mid-IR anisotropies can be quickly identified by cross-polarized IR-DCP polarimetry.

Keywords

Dual-comb spectroscopy, polarimetry, mid-infrared spectroscopy, nanofiber, anisotropy, sensing, infrared laser

Keypoints

- A novel dual-comb laser-based technique is established for polarization dependent mid-infrared spectroscopy
- Independent measurements of spectral s- and p-polarized transmission amplitudes and phases in the μs range
- Visualization of the anisotropy of nanofiber scaffolds as used for neural tissue applications.

Introduction

The anisotropy of materials is associated, for example, with direction dependent optical, mechanical, physical and chemical properties¹⁻⁷. Anisotropy plays a key role in optoelectronic, photonic, polymer, catalytic and bio-related research and applications. Specific examples are the design and engineering of optical devices¹⁻⁴, two-dimensional (2D) materials³, and touch-spun nanofibers for nerve regeneration⁷, the latter of which are studied in this work. For the analysis of anisotropic material properties, infrared (IR) methods are prominently used, as these probe material and structural properties in a contact-less manner in various environments with high sensitivity.

Driven by the tremendous application potential in scientific and industrial applications, numerous IR spectroscopies were developed in recent years. Classical IR spectroscopies are workhorses in many labs. However, it is not possible to simultaneously measure the real and imaginary part of complex transmissions or reflections. To satisfy this demand, polarimetric or ellipsometric IR spectroscopic methods have to be developed for the respective application fields. This challenge can be solved by introducing innovative measurement concepts, implementing new radiation sources, and realizing novel hyperspectral or imaging measurement schemes.

Recent rapidly developing IR spectroscopic methods based on quantum cascade lasers (QCLs) are heralding a new era in IR spectroscopic analytics with a plethora of new applications far beyond the possibilities of FTIR spectroscopy⁸⁻¹⁷. These methods nowadays offer high spectral resolutions in laboratory and field applications while providing high optical throughput, sub-mm spot sizes, and sub-s temporal resolution for sensing applications, time-resolved studies, as well as hyperspectral imaging. Of particular interest for structural and chemical analysis of interfaces, aggregates, thin films, and structured materials are polarization dependent QCL-based methods such as AFM-IR^{18,19}, IR nanoscopy²⁰, antenna-assisted IR nano-spectroscopy²¹, IR

microscopy^{22,23}, polarimetric IR-ATR²⁴, vibrational circular dichroism²⁵, far-field optical photothermal IR (O-PTIR)²⁶, and IR spectroscopic ellipsometry/polarimetry^{10,11,27-29}.

In 2016/2017, the dual-comb spectroscopic technique³⁰ was combined with polarization dependent measurements^{31,32}. So-called dual-comb ellipsometry³² in the near-IR spectral range of 1514–1595 nm became available. The authors³² already anticipated a transfer of the method to the mid-IR and far-IR region, which would enable future applications for studies of materials with vibrational transitions. In this work, we fulfill these expectations and introduce QCL-based IR dual-comb polarimetry (IR-DCP) as a novel technique for temporally (sub-ms) and spectrally (1.4 cm^{-1}) highly resolved investigations of anisotropic sample properties in the mid-IR spectral range.

Polarimetric methods

Figure 1 shows schematic designs of IR-DCP (a) and classical FTIR polarimetry (b). Both methods aim to probe the polarization dependent complex transmission (reflection) coefficients $t_{xy} = |t_{xy}| \cdot \exp(i \Delta_{xy})$, which describe the progression of incoming y-polarized light into x-polarized light. Both methods are sensitive to the transmission $T_{xy} = |t_{xy}|^2$. Classical FTIR polarimetry can acquire relative phase differences for two sets of polarization configurations, such as $\Delta_{xx} - \Delta_{yy}$. For FTIR polarimetric studies of materials with $\cos \Delta \approx 1$ (Δ close to 0 or π), a retarder is required as an additional optical element to achieve sufficiently high accuracy. In contrast, IR-DCP can directly measure absolute phases Δ_{xy} .

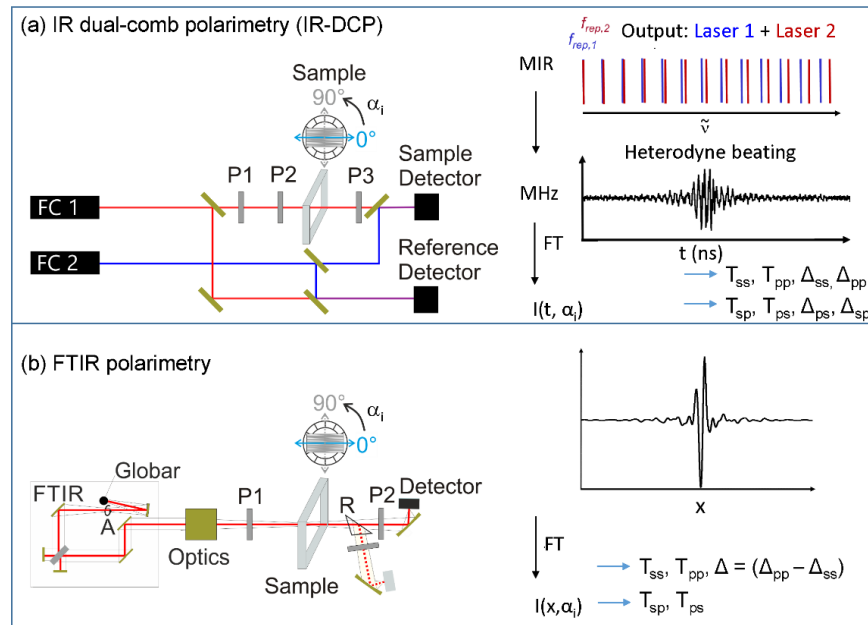


Figure 1 . Schematic set-ups of (a) IR dual-comb polarimetry (IR-DCP) and (b) FTIR polarimetry. The measurement principle is outlined on the right side. Typical measurement parameters are parallel-polarized (ss, pp) and cross-polarized (sp, ps) transmission T (reflection R) and absolute/relative phases Δ in dependence of the azimuthal angle (α_i). See text for further methodical details.

The dual-comb system (IRis-F1, IRsweep AG, Switzerland, schematic in Fig. 1(a)) comprises two QCL frequency combs (FC 1 and FC 2). FC 1 probes the sample, whereas FC 2 works as the local oscillator. Polarizers (P1, P2, P3) and beamsplitters (BaF₂, Specac, England) are used for controlling incident and output power and polarization states, as well as beam propagation and recombination. P1 regulates the incident power (typically about 0.75 mW at the sample), P2 sets the incident polarization, and P3 acts as an analyzer. Further polarizers (not shown) control the power incident on the reference detector and ensure

polarization matching of local oscillator beam and sample beam. The sample was placed between P2 and P3 on a rotational mount. The beam diameter at the sample position was about 3 mm (FWHM, Gauss).

The operating principles of dual-comb spectroscopy have been described previously³³⁻³⁵. Briefly, FC 1 and FC 2 deliver frequency combs with inter-line spacings ($f_{rep,1}$ and $f_{rep,2}$) of about 10 GHz. When FC 1 and FC 2 are overlaid on a high-bandwidth mercury-cadmium-telluride (MCT) detector, a heterodyne beating corresponding to $\Delta f_{rep} = f_{rep,1} - f_{rep,2}$ [?] 2 MHz can be recorded in the time-domain. Conducting a Fourier transform on this signal allows for the individual frequency contributions to be resolved. The reference detector is used to correct for amplitude and frequency noise of the free-running QCLs. For a given polarizer configuration, measuring the difference between a set-up without and one with a sample gives the complex transmission t_{xy} , the angle of which yields the absolute phase. The theoretical time resolution is $1/\Delta f_{rep}$ ^{35,36} however, for data-handling and signal-to-noise reasons, the spectrometer is typically operated at a time resolution of 4 μ s^{35,36}. In the present study, the integration time was 65 μ s. A transmission geometry at 0° incidence angle was used. For universality reasons, and to avoid confusion with the sample azimuthal settings in degrees (0° = horizontal orientation; 90° = vertical orientation), we use the following notation for polarizer/analyzer settings: (i) ss for parallel polarizers in horizontal direction, (ii) pp for parallel polarizers in vertical direction, (iii) sp and ps for crossed polarizers. Note that, for non-depolarizing samples, the ss-, pp-, sp- and ps-polarized measurements are directly related to the Jones matrix and specific combinations of the respective Mueller-matrix elements,³⁷ which enables the analysis of complex dielectric functions (real and imaginary part).³⁸

The FTIR polarimeter (Fig. 1(b)) is coupled to an FTIR IFS 55 spectrometer (BRUKER, Germany) serving as a radiation source. A Jacquinot aperture (A) of 1.85 mm results in a spot size on the sample of about 4.5 mm (FWHM). The sample was placed on a rotational mount. Polarizers (KRS5, Specac, England) P1 and P2 act as polarizer and analyzer, respectively. A liquid-nitrogen-cooled photovoltaic MCT detector (Kolmar Technologies, USA) was used. A retarding element (R) was additionally inserted for sensitive phase measurements. The opening angle was about $\pm 3.5^\circ$. Measured experimental quantities are the relative phase $\Delta = \Delta_{pp} - \Delta_{ss}$ and the polarization dependent transmission $T_{pp} = |t_{pp}|^2$ and $T_{ss} = |t_{ss}|^2$ at 0° incidence angle. $|t_{pp}|$ and $|t_{ss}|$ represent the amplitudes of the respective pp- and ss-polarized complex transmission coefficients (for incidence angles larger than 0°, pp is parallel and ss is perpendicular to the optical incidence plane), and Δ is the phase shift between them. Further details are found in Refs.^{38,39} for the ellipsometric method and in Ref.³⁹ for the employed set-up.

Materials

A nanofiber scaffold was prepared via the touch-spinning method in a free-standing manner on a wire collector from 8% polycaprolactone (PCL, $M_n = 80,000$ g/mol, Sigma-Aldrich) in chloroform (ACS grade, VWR Chemicals BDH). Details on touch-spinning can be found in Ref.⁷. The fibers were exposed to a 0.1% bovine serum albumin (BSA) solution.

Anisotropic nanofiber scaffold

Figure 2 shows polarization dependent transmission and phase spectra of the nanofiber sample for 0° and 90° azimuthal rotation. The observed band at about 1240 cm^{-1} is assigned to the asymmetric C–O–C stretching vibration (according to Ref.⁴⁰) of the PCL chain. The onset of a second vibrational band at about 1293 cm^{-1} is observed at the edge of the investigated spectral range. Qualitative and quantitative agreement in band position, amplitude and shape is found between the corresponding sets of polarized transmission IR-DCP and FTIR polarimetric spectra. A strong anisotropy is identified in the range of the C–O–C vibrational band. This anisotropy originates from the direction-dependent vibrational absorption due to the predominant alignment of polymer chains within single fibers, but also due to the overall close-to-parallel orientation of the individual fibers^{41,42}. Qualitative agreement is observed between the relative phase difference spectra obtained from IR-DCP and FTIR polarimetry (Fig. 2(b)).

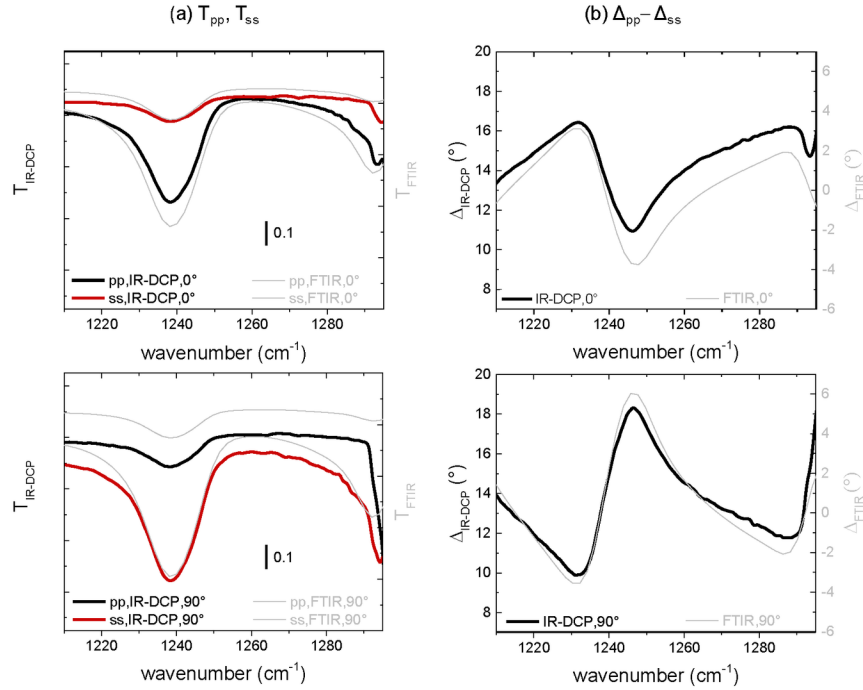


Figure 2. (a) T_{pp} and T_{ss} from IR-DCP and FTIR polarimetry at 0° (top) and 90° (bottom) azimuthal sample rotation. (b) Corresponding polarized phase-difference spectra from IR-DCP and FTIR polarimetry.

The band amplitudes in the IR-DCP transmission and phase spectra at 0° azimuthal angle are slightly larger compared to FTIR. Such differences could be related to the inhomogeneity of the fiber scaffold and the different sizes and opening angles of the probe beam in DCP and FTIR. However, band positions and shapes agree well for both methods. Indeed, the relative phase spectra exhibit the expected Kramers–Kronig consistent line shape, thus demonstrating the validity of the method.

The recorded IR-DCP and FTIR polarimetric phases show a constant offset of approximately 13°. Its likely origin is the adjustment of incident power via P1 between the Δ_{pp} and Δ_{ss} measurements necessitated by a change in the input polarization. For future measurements, an invariant P1 is recommended, for example, by setting P1 to 45° and controlling the power through neutral density filters.

Figure 3 (a) shows images of ss- and sp-polarized transmission and absolute phase spectra versus sample azimuth in 10° steps. Maximum band intensities in the T_{ss} images are observed around 90° azimuth, whereas vanishing band intensities in T_{sp} are seen at 0° and 90° azimuth. The average orientation of transition dipole moments of the related C–O–C vibrational band is therefore aligned predominantly in the direction of the fibers, in agreement with the overall predominant alignment of the fibers in the scaffold.

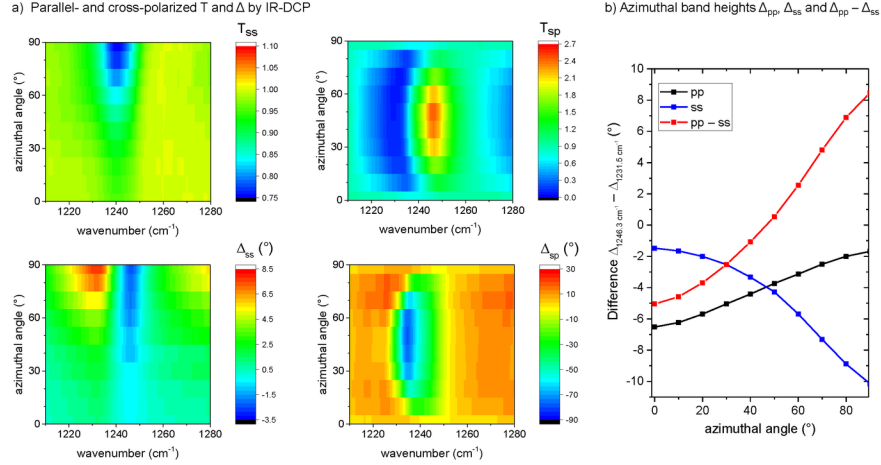


Figure 3. a) Images of azimuthal ss- and sp-polarized IR-DCP transmission and absolute phase spectra. T_{sp} exhibits a baseline value of 1 in the absence of anisotropy (e.g., for azimuthal sample rotations of 0° and 90°) due to the spectral normalization to a measurement without a sample. b) Azimuthal variation of the C–O–C band height in the absolute ss- and pp-polarized phases as well as their difference.

The parallel-polarized T_{ss} and Δ_{ss} images capture all vibrational contributions along the ss polarization axis and therefore also include isotropic contributions. In contrast, the cross-polarized T_{sp} and Δ_{sp} images are only sensitive to signals from anisotropic contributions, qualifying them for the direct inspection of anisotropies. The anisotropic absorption behavior of the nanofibers is directly identified in the cross-polarized images, which show band maxima at 45° azimuthal angle, in agreement with maximum in-plane p–s anisotropy for aligned nanofibers. The parallel-polarized Δ_{ss} phase image shows azimuthally homogeneous areas beside the vibrational band contributions, which could potentially be used as a measure of optical thickness.

Figure 3 (b) shows the azimuthal variation of the C–O–C band heights in the ss- and pp-polarized phase spectra as well as their difference. Classical FTIR polarimetry cannot measure absolute phases, but only relative ones. In contrast, IR-DCP can separate the information encoded in the polarization-dependent absolute phases.

In summary, the spectral polarimetric amplitudes and phases simultaneously provide complementary information on sample structure and thickness. Moreover, IR-DCP acquires absolute phase data for arbitrary polarization configurations, allowing, for instance, the direct measurement of Δ_{sp} without the need for rotating optical elements such as polarizers. Fast sample imaging applications of parallel- and cross-polarized band amplitude and phase properties thus become available in the mid-IR spectral range.

Time characteristics

Figure 4 (a) shows a time sequence of transmission and absolute phase spectra for the fiber scaffold obtained at a specific and constant polarimetric measurement setting (pp configuration at 45° sample azimuth).

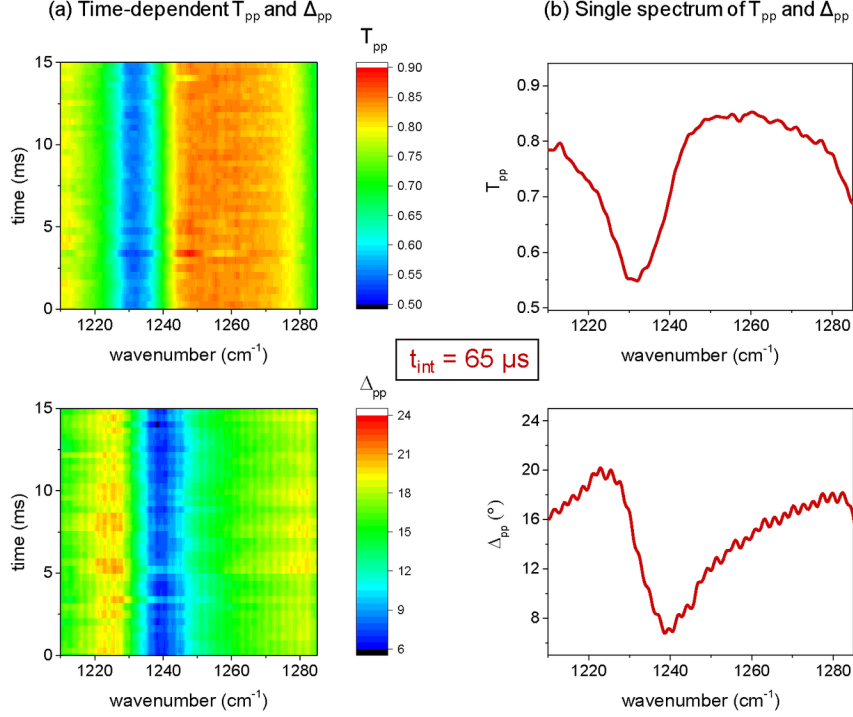


Fig. 4. a) Images of time dependent T_{pp} and Δ_{pp} spectra of the fiber scaffold at 45° azimuth. (b) The first single transmission and absolute phase spectrum with $65 \mu s$ integration time (t_{int}). The spectral resolution is 1.4 cm^{-1} .

These time dependent images prove the high stability and robustness of the method in the shown time range for both transmission and absolute phase measurements. The integration time of a single spectrum (see Fig. 5(b)) is $65 \mu s$, plus a shot-to-shot delay of ca. $210 \mu s$, giving a non-stroboscopic time resolution of ca. $275 \mu s$. The time resolution can be pushed to as low as $1 \mu s$ with a zero shot-to-shot delay, with a tradeoff of limiting the maximum measurement duration to 256 ms . The noise of the DCS spectrometer in the second to sub-second time regime scales with the inverse of the square root of integration time⁴³; the signal-to-noise can therefore be improved by averaging multiple spectra.

With its high time resolution for spectral monitoring in broad time windows from the min to μs range (with the potential of sub-microsecond time resolution⁴³), IR-DCP is currently a few orders of magnitude faster than reported for QCL-based IR laser polarimetry ([?] $100 \text{ ms} / 100 \text{ cm}^{-1}$)³³.

Conclusion and outlook

Infrared dual-comb polarimetry was introduced as a new polarimetric technique for studies of anisotropic samples in the mid-IR spectral range. IR-DCP enables mid-IR polarimetric measurements of amplitudes and absolute phases at high spectral resolution (1.4 cm^{-1}). The method was applied to characterize a nanofiber scaffold with strong in-plane anisotropy. Azimuthal images of parallel- and cross-polarized dual-comb spectra were proven to be applicable for direct inspection of anisotropic vibrational properties. Having with a single polarizer configuration access to both amplitudes and absolute phases offers new imaging prospects for cross-polarized sample properties.

Furthermore, IR-DCP provides sub-millisecond measurement times of $275 \mu s$ or less (potentially even sub- μs). The accessible integration times are far below those achievable with conventional FTIR techniques, thus enabling future applications regarding sub-ms resolved spectral investigations of irreversible or non-cyclic variations of structural sample properties. The superior time resolution of IR-DCP compared with

other IR approaches renders the method potentially interesting for many applications in photonics such as process control in the fabrication of waveguides and functional metasurfaces. In general, the novel time-resolved polarimetric possibilities could have a high potential scientific impact for previously unfeasible *in situ* and *operando* studies of irreversible or noncyclic processes or sample modifications. Further future applications of IR-DCP will also become available in other polarimetric measurement geometries.

In summary the developed IR dual-comb polarimetric method has high potential for chemical and structural studies, e. g., of anisotropic samples, protein dynamics, phase transitions, chemical modifications and reactions, which is relevant for material science, catalysis, biophysics, photonics, rheology and metrology.

Notes The authors declare no conflicts of interest.

Data availability statement The data that support the findings of this study are available from the corresponding author upon reasonable request.

Acknowledgments

The authors thank T. Shaykhutdinov for his scientific input and I. Engler and Ö. Savas for technical support. Financial funding is acknowledged: Bundesministerium für Bildung und Forschung; Die Regierende Bürgermeisterin von Berlin – Senatsverwaltung Wissenschaft, Gesundheit, Pflege und Gleichstellung; Ministerium für Innovation, Wissenschaft und Forschung des Landes Nordrhein-Westfalen; Federal Ministry of Education and Research (CatLab 03EW0015A); European Union (EFRE 1.8/13, Horizon 2020 grant 820419).

References

1. He, M.; Folland, T. G.; Duan, J; Alonso-González, P.; De Liberato, S.; Paarmann, A; Caldwell, J. D. Anisotropy and Modal Hybridization in Infrared Nanophotonics Using Low-Symmetry Materials, *ACS Photonics* **2022**, *9*, 1078-1095. DOI: 10.1021/acsp Photonics.1c01486
2. Meng, Y., Chen, Y., Lu, L. *et al.* Optical meta-waveguides for integrated photonics and beyond. *Light Sci Appl* **2021**, *10*, 235. <https://doi.org/10.1038/s41377-021-00655-x>
3. Yang, H.; Jussila, H.; Autere, A.; Komsa, H.-P.; Ye, G.; Chen, X.; Hasan, T.; Sun, Z. Optical Waveplates Based on Birefringence of Anisotropic Two-Dimensional Layered Materials. *ACS Photonics* **2017**, *4*, 3023-3030. DOI: 10.1021/acsp Photonics.7b00507
4. Silva-Guillén, J. A.; Canadell, E.; Guinea, F.; Roldán, R. Strain Tuning of the Anisotropy in the Optoelectronic Properties of TiS₃. *ACS Photonics* **2018**, *5*, 3231-3237. DOI: 10.1021/acsp Photonics.8b00467
5. Valderrabano, M. Influence of Anisotropic Conduction Properties in the Propagation of the Cardiac Action Potential. *Prog. Biophys. Mol. Biol.* **2007**, *94*, 144–168.
6. Street, R. A. The Benefit of Order. *Nat. Mater.* **2006**, *5*, 171–172.
7. Lee, S.-J.; Asheghali, D.; Blevins, B.; Timsina, R.; Esworthy, T.; Zhou, X.; Cui, H.; Hann, S. Y.; Qiu, X.; Tokarev, A.; Minko, S.; Zhang, L. G. Touch-Spun Nanofibers for Nerve Regeneration. *ACS Appl. Mat. & Int.* **2020**, *12*, 2067-2075. DOI: 10.1021/acsam.9b18614
8. Vitiello, M.S.; Scalari, G.; Williams, B.; De Natale, P. Quantum cascade lasers: 20 years of challenges. *Opt. Express* **2015**, *23*, 5167–5182. DOI: 10.1364/OE.23.005167
9. Hugi, A; Horvath, R.; Jouy, P. Advances of dual-comb spectroscopy based on QCL for environmental and water analysis. *Proc. SPIE, Optical Fibers and Sensors for Medical Diagnostics, Treatment and Environmental Applications* **2021**, *XXI*, 1163511. DOI: 10.1117/12.2582911
10. Hinrichs, K.; Shaykhutdinov, T.; Kratz, C.; Furchner, A. Brilliant mid-infrared ellipsometry and polarimetry of thin films: Toward laboratory applications with laser based techniques. *J. Vac. Sci. & Technol. B* **2019**, *37*, 060801. DOI: 10.1116/1.5122869
11. Furchner, A.; Hinrichs, K. Mid-Infrared Laser Ellipsometry: A New Era Beyond FTIR. *Adv. Opt. Technol.* **2022**, Article ASAP. DOI: 10.1515/aot-2022-0013.
12. Akhgar, C.K.; Ramer, G.; Žbik, M.; Trajnerowicz, A.; Pawluczyk, J.; Schwaighofer, A.; Lendl, B. The Next Generation of IR Spectroscopy: EC-QCL-Based Mid-IR Transmission Spectroscopy of Proteins with Balanced Detection. *Analytical Chemistry* **2020**, *92*, 9901-9907. DOI:

- 10.1021/acs.analchem.0c01406
13. Schwaighofer, A.; Brandstetter, M.; Lendl, B. Quantum cascade lasers (QCLs) in biomedical spectroscopy. *Chem. Soc. Rev.* **2017** , *46* , 5903-5924. DOI: 10.1039/C7CS00403F
 14. Schönhals, A.; Kröger-Lui, N.; Pucci, A.; Petrich, W. On the role of interference in laser-based mid-infrared widefield microspectroscopy. *J. of Biophotonics* **2018** , *11* , e201800015. DOI: 10.1002/jbio.201800015
 15. Consolino, L.; Cappelli, F.; de Cumis, M. S.; De Natale, P. QCL-based frequency metrology from the mid-infrared to the THz range: a review. *Nanophotonics* **2019** , *8* , 181-204. DOI: 10.1515/nanoph-2018-0076
 16. Galán-Freyte, N. J.; Pacheco-Londoño, L. C.; Román-Ospino, A. D.; Hernandez-Rivera, S. P. Applications of Quantum Cascade Laser Spectroscopy in the Analysis of Pharmaceutical Formulations. *Appl. Spectr.* **2016** , *70* , 1511-1519. DOI: 10.1177/0003702816662609
 17. Wei, S.; Kulkarni, P.; Ashley, K.; Zheng, L. Measurement of Crystalline Silica Aerosol Using Quantum Cascade Laser-Based Infrared Spectroscopy. *Sci. Rep.* **2017** , *7* , 13860. DOI: 10.1038/s41598-017-14363-3
 18. Hinrichs, K.; Shaykhutdinov, T. Polarization-Dependent Atomic Force Microscopy–Infrared Spectroscopy (AFM-IR): Infrared Nanopolarimetric Analysis of Structure and Anisotropy of Thin Films and Surfaces. *Appl. Spectr.* **2018** , *72* , 817-832. DOI: 10.1177/0003702818763604
 19. Dazzi, A.; Prater, C. B. AFM-IR: Technology and Applications in Nanoscale Infrared Spectroscopy and Chemical Imaging. *Chem. Rev.* **2017** , *117* , 5146-5173. DOI: 10.1021/acs.chemrev.6b00448
 20. Wehmeier, L.; Lang, D.; Liu, Y.; Zhang, X.; Winnerl, S.; Eng, L. M.; Kehr, S. C. Polarization-dependent near-field phonon nanoscopy of oxides: SrTiO₃, LiNbO₃, and PbZr_{0.2}Ti_{0.8}O₃. *Phys. Rev. B* **2019** , *100* , 035444. DOI: 10.1103/PhysRevB.100.035444
 21. Yao, Z.; Chen, X.; Wehmeier, L.; Xu, S.; Shao, Y.; Zeng, Z.; Liu, F.; Mcleod, A. S.; Gilbert Corder, S. N.; Tsuneto, M.; Shi, W.; Wang, Z.; Zheng, W.; Bechtel, H. A.; Carr, G. L.; Martin, M. C.; Zettl, A.; Basov, D. N.; Chen, X.; Eng, L. M.; Kehr, S. C.; Liu, M. Probing subwavelength in-plane anisotropy with antenna-assisted infrared nano-spectroscopy. *Nat. Commun.* **2021** , *12* , 2649. DOI: 10.1038/s41467-021-22844-3
 22. Tong, L.; Huang, X.; Wang, P.; Ye, L.; Peng, M.; An, L.; Sun, Q.; Zhang, Y.; Yang, G.; Li, Z.; Zhong, F.; Wang, F.; Wang, Y.; Motlag, M.; Wu, W.; Cheng, G. J.; Hu, W. Stable mid-infrared polarization imaging based on quasi-2D tellurium at room temperature. *Nat Commun.* **2020** , *11* , 2308. DOI: 10.1038/s41467-020-16125-8
 23. Xu, S.; Rowlette, J.; Lee, Y. J. Imaging 3D molecular orientation by orthogonal-pair polarization IR microscopy. *Opt. Express* **2022** , *30* , 8436-8447. DOI: 10.1364/OE.449667
 24. Freitag, S.; Baer, M.; Buntzoll, L.; Ramer, G.; Schwaighofer, A.; Schmauss, B.; Lendl, B. Polarimetric Balanced Detection: Background-Free Mid-IR Evanescent Field Laser Spectroscopy for Low-Noise, Long-term Stable Chemical Sensing. *ACS Sensors* **2021** , *6* , 35-42. DOI: 10.1021/acssensors.0c01342
 25. Ludeke, S.; Pfeifer, M.; Fischer, P. Quantum-cascade laser based vibrational circular dichroism. *J. Am. Chem. Soc.* **2011** , *133* , 5704-5707. DOI: 10.1021/ja200539d
 26. Bakir, G.; Girouard, B. E.; Wiens, R.; Mastel, S.; Dillon, E.; Kansiz, M.; Gough, K. M. Orientation Matters: Polarization Dependent IR Spectroscopy of Collagen from Intact Tendon Down to the Single Fibril Level. *Molecules* **2020** , *25* , 4295. DOI: 10.3390/molecules25184295
 27. Furchner, A.; Kratz, C.; Rappich, J.; Hinrichs, K. Multi-Timescale Infrared Quantum Cascade Laser Ellipsometry. *Opt. Lett.* **2022** , *47* , 2834-2837. DOI: 10.1364/OL.457688
 28. Ebner, A.; Zimmerleiter, R.; Hingerl, K.; Brandstetter, M. Towards Real-Time In-Situ Mid-Infrared Spectroscopic Ellipsometry in Polymer Processing. *Polymers* **2022** , *14* , 7. DOI: 10.3390/polym14010007
 29. Furchner, A.; Kratz, C.; Hinrichs, K. Sub-second infrared broadband-laser single-shot phase-amplitude polarimetry of thin films. *Opt. Lett.* **2019** , *44* , 4387-4390. DOI: 10.1364/OL.44.004387
 30. Picqué, N.; Hänsch, T. W. Frequency comb spectroscopy. *Nature Photon* **2019** , *13* , 146-157. DOI: 10.1038/s41566-018-0347-5

31. Sumihara, K.A.; Okubo, S.; Okano, M.; Inaba, H.; Watanabe, S. Polarization-sensitive dual-comb spectroscopy. *J. Opt. Soc. Am. B* **2017** , *34* , 154-159. DOI: 10.1364/JOSAB.34.000154
32. Minamikawa, T.; Hsieh, Y. D.; Shibuya, K.; Hase, E.; Kaneoka, Y.; Okubo, S.; Inaba, H.; Mizutani, Y.; Yamamoto, H.; Iwata, T.; Yasui T. Dual-comb spectroscopic ellipsometry. *Nat. Commun.* **2017** , *8* , 610. DOI: 10.1038/s41467-017-00709-y
33. Villares, G.; Hugi, A.; Blaser, S.; Faist, J. Dual-comb spectroscopy based on quantum-cascade-laser frequency combs. *Nat. Commun.* **2014** , *5* , 5192. DOI: 10.1038/ncomms6192
34. Coddington, I.; Newbury, N.; Swann, W. Dual-comb spectroscopy. *Optica* **2016** , *3* , 414-426. DOI: 10.1364/OPTICA.3.000414
35. Norahan, M. J.; Horvath, R.; Woitzik, N.; Jouy, P.; Eigenmann, F.; Gerwert, K.; Kötting, C. Microsecond-Resolved Infrared Spectroscopy on Nonrepetitive Protein Reactions by Applying Caged Compounds and Quantum Cascade Laser Frequency Combs. *Anal. Chem.* **2021** , *93* , 6779-6783. DOI: 10.1021/acs.analchem.1c00666
36. Pinkowski, N. H.; Biswas, P.; Shao, J.; Strand, C. L.; Hanson, R. K. Thermometry and speciation for high-temperature and -pressure methane pyrolysis using shock tubes and dual-comb spectroscopy. *Meas. Sci. Technol.* **2021** , *32* , 125502.
37. Muñoz-Pineda, E.; Järrendahl, K.; Arwin, H.; Mendoza-Galván, A. Symmetries and relationships between elements of the Mueller matrix spectra of the cuticle of the beetle *Cotinis mutabilis*. *Thin Sol. Films* **2014** , 571, 660-665. DOI: 10.1016/j.tsf.2013.11.144
38. Hinrichs, K.; Eichhorn, K.-J. Chap. 1, 2, 3, 6, 7, 9, 12, 13, 19, 20, 21, 22 in *Ellipsometry of Functional Organic Surfaces and Films* , 2nd ed., Springer Ser. Surf. Sci. *52* , Springer International Publishing AG, 2018.
39. Chalmers, J.M., Griffiths, P.R. eds.; A. Röseler, E.H. Korte, Chap. 2.8 in *Handbook of Vibrational Spectroscopy* ; John Wiley & Sons, Ltd, 2001.
40. Gorodzha, S. N.; Surmeneva, M. A.; Surmenev, R. A. Fabrication and characterization of polycaprolactone cross-linked and highly-aligned 3-D artificial scaffolds for bone tissue regeneration via electrospinning technology. *Mat. Sci. Eng.* **2015** , *98* , 012024. DOI: 10.1088/1757-899X/98/1/012024
41. Hinrichs, K.; Blevins, B.; Furchner, A.; Yadavalli, N. S.; Minko, S. Infrared polarimetry: Anisotropy of polymer nanofibers. *Micro and Nano Engineering* **2022** , *14* , 100116. DOI: 10.1016/j.mne.2022.100116
42. Wang, Z.; Sun, B.; Lu, X.; Wang, C.; Su, Z. Molecular Orientation in Individual Electrospun Nanofibers Studied by Polarized AFM-IR. *Macromolecules* **2019** , *52* , 9639-9645. DOI: 10.1021/acs.macromol.9b01778
43. Klocke, J. L.; Mangold, M.; Allmendinger, P.; Hugi, A.; Geiser, M.; Jouy, P.; Faist, J.; Kottke, T. Single-Shot Sub-microsecond Mid-infrared Spectroscopy on Protein Reactions with Quantum Cascade Laser Frequency Combs. *Anal. Chem.* **2018** , *90* , 10494-10500. DOI: 10.1021/acs.analchem.8b02531